ASPS Conference Proceedings 1: 1817-1822 (2022)

Proceedings of

12th Structural Engineering Convention-An International Event (SEC 2022)

Available at https://asps-journals.com/index.php/acp

On Effects of Shear Deformation on the Static Pull-in Instability Behaviour of Narrow Rectangular Timoshenko Microbeams

Kedar S. Pakhare [1, *], Punith P.[1], P.J. Guruprasad [1], Rameshchandra P. Shimpi [1]

[1] Department of Aerospace Engineering, Indian Institute of Technology Bombay, Mumbai 400 076, India

Paper ID - 290081

Abstract

MEMS devices utilize electrostatics as preferred actuation method. The accurate determination of pull-in instability parameters (*i.e.*, pull-in voltage and pull-in displacement) of such devices is critical for their correct design. It should be noted that similar to parallel plate capacitors, the electrostatic force between the surface of the deformable microbeam and stationary ground is non-linear in nature. Hence the analysis associated with *MEMS* devices is always inherently non-linear. In the literature, these devices have been majorly analyzed as Bernoulli-Euler microbeams with cantilever or clamped-clamped beam end conditions. However, Dileesh et al. (doi: 10.1115/ESDA2012-82536) have studied the static and dynamic pull-in instability behavior of slender cantilever microbeams by developing a six-nodded spectral finite element based on the Timoshenko beam theory (*TBT-SFE*). They have demonstrated the accuracy of the *TBT-SFE* by comparing their results with corresponding results of *COMSOL*-based three-dimensional finite element simulations. In addition, effects of shear deformation also start to play significant role as the beam thickness-to-length ratio increases. In this paper, authors have developed the *TBT-SFE* based on the work by Dileesh et al. for the case of statics. However, unlike Dileesh et al. where they have developed a six-nodded *TBT-SFE*, authors have investigated the best combination of number of nodes per element and total number of elements to carry out the study. For this purpose, authors have first calculated results of the maximum beam transverse displacement, for a shear deformable propped-cantilever microbeam under the action of uniformly distributed transverse load, obtained by utilizing the developed *TBT-SFE* with different combinations of number of nodes per element and total number of elements. These results are then compared with corresponding analytical results available in the literature to arrive at the best combination of number of nodes per element and total number of elements for the electrostatic-elastic analysis. In the second step, the finalized *TBT-SFE* is utilized to determine static pull-in instability parameters of narrow microbeams with various fixity conditions and beam thickness-to-length ratios. This study highlights the importance of transverse shear effects on pull-in instability parameters of Timoshenko microbeams.

Keywords: *MEMS*, Microbeams, Pull-in Instability, Beam Transverse Shear Deformation, Timoshenko Beam Theory, Spectral Finite Element

1. Introduction

Micro-Electro-Mechanical Systems (*MEMS*) are being used in devices such as actuators, resonators and switches. Various actuation methods such as piezoelectric, electromagnetic or electrostatics can be used for operating *MEMS*. Out of which, the electrostatics is used as a preferred method for *MEMS* operation because of their higher energy density, lower power requirements and ease in microfabrication process (references [1, 2]).

Most often, these systems are analysed as a unit comprising of a deformable microbeam and ground electrode. Just like in the case of parallel plate capacitors, the electrostatic force between the surface of the deformable microbeam and stationary ground for any applied voltage is non-linear *i.e.*, it depends on an inverse of the square of the distance between two electrodes. However, the restoring force associated with the deformed microbeam is linear *i.e.*, it depends on the amount of deformation that the microbeam undergoes under the action of an electrostatic force. As a result of this mismatch in two forces, the microbeam has an inherent upper limit on the amount of voltage that can be applied between two electrodes. If the applied voltage exceeds this critical value, the microbeam cannot resist the electrostatic force acting on it with its own restoring force. This causes a sudden collapse of the deformable microbeam on the stationary ground. The just-mentioned phenomenon is referred to as 'the pull-in instability' in the literature. The voltage and microbeam deformation at which the pull-in instability kicks in is referred to as the pull-in voltage and pull-in displacement respectively (Nathanson et al. [3]).

In addition, beam transverse shear deformation effects, which are negligible for slender beams, become considerable for thick / shear deformable beams. In order to incorporate effects of the transverse shear in the beam deformation, various displacement-based first-order shear deformation beam theories (*FSDT*s) and higher-order shear deformation beam theories (*HSDT*s) have been proposed in the literature (Ghugal and Shimpi [4]). *FSDT*s as well as *HSDT*s try to address drawbacks of the Bernoulli-Euler beam theory (*BEBT*) which does not account for the beam transverse shear deformation as a result of its assumed

*Corresponding author. Tel: +919867005668; E-mail address: kedar188200@gmail.com

Published online: December 19, 2022

doi:10.38208/acp.v1.723

displacement field. The primary assumption with regard to *FSDT*s is that the straight line, which is normal to the undeformed beam neutral axis, remains straight but may or may not remain normal to the deformed beam neutral axis. As a result, *FSDT*s result in the constant transverse shear strain (and hence the constant transverse shear stress) through the beam thickness. Hence *FSDT*s require a shear correction factor while satisfying the constitutive relation relating the beam transverse shear stress with the beam transverse shear strain. Whereas, the primary assumption with regard to *HSDT*s is that the straight line, which is normal to the undeformed beam neutral axis, may or may not remain straight and may or may not remain normal to the deformed beam neutral axis. As a result, *HSDT*s result in the nonlinear variation of the transverse shear strain (and hence the nonlinear variation of the transverse shear stress) through the beam thickness. *HSDT*s do not require a shear correction factor while satisfying the constitutive relation relating the beam transverse shear stress with the beam transverse shear strain. As compared to *FSDT*s, *HSDT*s generally involve increased number of primary unknowns and require the specification of increased number of beam end conditions.

Majority of the work on an electrostatic-elastic analysis of microbeams reported in the literature use the *BEBT*. However, Dileesh et al. [5] have studied the static and dynamic pull-in instability behavior of slender cantilever microbeams by developing a six-nodded spectral finite element based on the Timoshenko beam theory (*TBT-SFE*, references [6, 7]). They have demonstrated the accuracy of the *TBT-SFE* by comparing their results pertaining to slender microbeams with corresponding results of *COMSOL*-based three-dimensional finite element simulations.

In this paper, the *TBT-SFE* is reformulated based on the work by Dileesh et al. [5] for the case of statics. However, the investigation of the best combination of number of nodes per element and total number of elements is carried out. For this purpose, authors have first calculated results of the maximum beam transverse displacement, for a shear deformable propped-cantilever microbeam under the action of uniformly distributed transverse load, obtained by utilizing the developed *TBT-SFE* with different combinations of number of nodes per element and total number of elements. These results are then compared with corresponding analytical results of Pakhare et al. [8] to arrive at the best combination of number of nodes per element and total number of elements for the electrostatic-elastic analysis. In the second step, the finalized *TBT-SFE* is utilized to determine static pull-in instability parameters of narrow microbeams with various fixity conditions and beam thickness-to-length ratios. This paper aims to highlight the impact of transverse shear deformation effects on pull-in instability parameters of narrow Timoshenko microbeams which has not been, to the best of authors' knowledge, addressed in the literature.

2. Theoretical Details of the *TBT-SFE*

An electrostatically actuated narrow shear deformable microbeam in a cantilever form is as shown in Fig. 1.

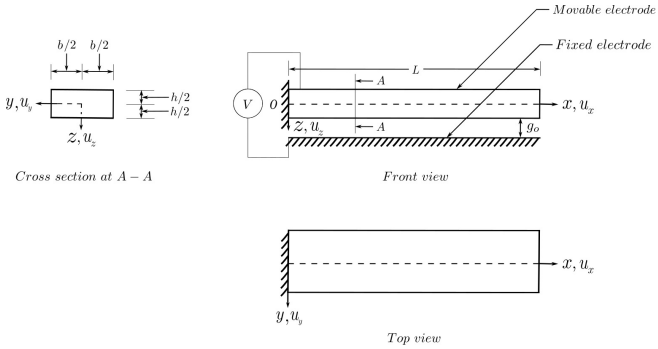

Fig. 1. An electrostatically actuated narrow shear deformable cantilever microbeam.

Governing equations of the *TBT* (Dileesh et al. [5]) for the case of statics are as follows:

$$G\,A\,\kappa\left(\frac{d^2w}{dx^2}+\frac{d\phi}{dx}\right)+q=0 \tag{1}$$

$$E\,I\,\frac{d^2\phi}{dx^2}-G\,A\,\kappa\left(\frac{dw}{dx}+\phi\right)=0 \tag{2}$$

Where symbols in Eqs. 1 and 2 have the same meaning as those used in Dileesh et al. [5]. Here, w and Φ represent primary unknowns of the *TBT*.

Physically meaningful beam end conditions of the *TBT* with regard to the beam end $x = 0$, and can be defined at the beam end $x = L$ based on a similar logic, for an illustrative purpose are as follows:

- When the beam end $x = 0$ is simply-supported:

$$[w]_{x=0}=0 \tag{3}$$

$$\left[\frac{d^2\phi}{dx^2}\right]_{x=0}=0 \tag{4}$$

- When the beam end $x = 0$ is clamped:

$$[w]_{x=0}=0 \tag{5}$$

$$[\phi]_{x=0}=0 \tag{6}$$

- When the beam end $x = 0$ is free:

$$\left[\frac{d^2\phi}{dx^2}\right]_{x=0}=0 \tag{7}$$

$$\left[\frac{dw}{dx}+\phi\right]_{x=0}=0 \tag{8}$$

Appropriate beam end conditions are chosen from Eqs. 7 through 8 for illustrative examples considered in this paper.

Patera [9] have introduced the spectral element method (*SEM*) with regard to problems pertaining to the computational fluid dynamics. Just like a regular finite element technique (*FEM*), the *SEM* is also a weighted residual technique. However, the *SEM* utilizes Lagrange interpolating polynomials (*LIP*s) of higher order along with Gauss-Lobatto-Legendre (*GLL*) integration points. Hence the *SEM* combines advantages of the *FEM* along with an exponential convergence of global spectral methods.

Unlike the *FEM* where nodes of an element are generally spaced evenly, nodes of an element of the *SEM* are not evenly spaced. A one-dimensional spectral element with 4 and 6 nodes along with their corresponding *LIP*s of order 3 and 5 respectively are shown in Fig. 2 and Fig. 3 respectively.

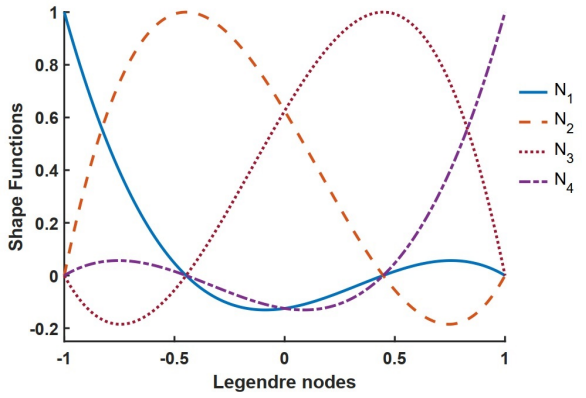

Fig. 2. A 4-noded spectral element and corresponding Lagrange interpolating polynomials of degree 3.

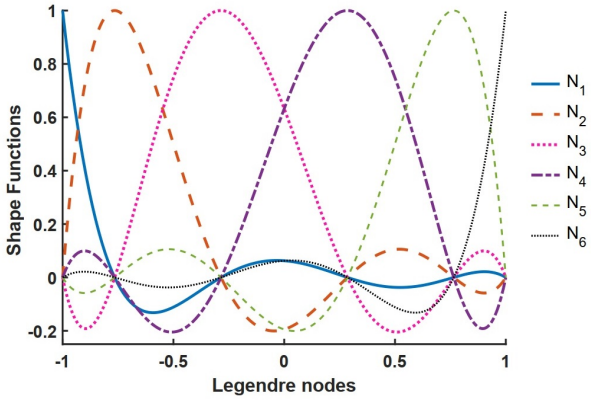

Fig. 3. A 6-noded spectral element and corresponding Lagrange interpolating polynomials of degree 5.

Where locations of these nodes are same as the location of *GLL* integration points, and are given by roots of the following expression:

$$\left(1 - \xi^2\right) F_p^{'}(\xi) = 0 \tag{9}$$

With $F^{'}_p$ is a first derivative of the Legendre polynomial of degree p (Komatitsch and Vilotte [10]).

In this paper, *LIP*s used for the geometrical mapping are the same as those used to discretise primary variables of the *TBT*. For a physical beam element having $p + 1$ nodes, this discretisation of the physical coordinate and primary variables is as follows:

$$\begin{aligned} x &= \sum_{i=1}^{p+1} N_i \, \bar{x}_i \\ w(\xi) &= \sum_{i=1}^{p+1} N_i \, \bar{w}_i \\ \phi(\xi) &= \sum_{i=1}^{p+1} N_i \, \bar{\phi}_i \end{aligned} \tag{10}$$

Where N_i represents a *LIP* of degree p, the expression for which is as follows:

$$N_i(\xi) = \prod_{\substack{i=1 \\ i \neq j}}^{p+1} \frac{\xi - \xi_j}{\xi_i - \xi_j}$$

Here, a physical beam element of length 'L' is mapped into a reference beam element with ξ as its coordinate which spans $-1 \leq \xi \leq 1$. Any integration of a function in the reference element is carried out as follows:

$$\int_{\Delta} g(x)\, dx = \int_{-1}^{1} g(\xi)\, J(\xi)\, d\xi \tag{10}$$

Where J is the Jacobian of an elemental transformation.

After performing the standard finite element formulation procedure (Reddy [11]), elemental equations are obtained as follows:

$$\begin{bmatrix} K_{ww} & (K_{\phi w})^T \\ K_{\phi w} & K^B{}_{\phi\phi} + K^S{}_{\phi\phi} \end{bmatrix} \begin{Bmatrix} \bar{w} \\ \bar{\phi} \end{Bmatrix} = \begin{Bmatrix} \bar{q} \\ \bar{0} \end{Bmatrix} \tag{11}$$

With

$$\begin{aligned} K_{ww} &= G\,\kappa\,A \int_{-1}^{1} \frac{dN^T}{d\xi} \frac{dN}{d\xi} J^{-1}\, d\xi \\ K_{\phi w} &= G\,\kappa\,A \int_{-1}^{1} \frac{dN^T}{d\xi} N\, d\xi \\ K^B{}_{\phi\phi} &= E\,I \int_{-1}^{1} \frac{dN^T}{d\xi} \frac{dN}{d\xi} J^{-1}\, d\xi \\ K^S{}_{\phi\phi} &= G\,\kappa\,A \int_{-1}^{1} N^T\, N\, J\, d\xi \end{aligned} \tag{12}$$

And the consistent load vector is given as follows:

$$\bar{q} = \int_{-1}^{1} N^T\, q(\xi)\, J\, d\xi \tag{13}$$

For the microbeam applied by a uniformly distributed transverse loading

$$q(\xi) = q_o \tag{14}$$

Where q_o is the amplitude of the applied transverse loading.

For the microbeam under the action of the electrostatic force (without considering effects of the fringing field)

$$q(\xi) = \frac{\varepsilon_o\, b\, V^2}{2\left(g_o - w(\xi)\right)^2} \tag{15}$$

The non-linear *SE* electrostatic-elastic analysis is carried out using the Picard's iterative method (Dileesh et al. [5]). The prescribed tolerance for the same is taken as 0.000001. It should be noted that as the developed *TBT-SFE* utilizes higher-order *LIP*s, it is free from shear locking phenomenon and subsequent shear locking related issues.

3. Illustrative Examples, Numerical Results and Discussion

In the first step, the developed *TBT-SFE* is utilized to find out the maximum non-dimensional beam transverse displacement ($w^*_{max} = (100\, w_{max}\, E\, I) / (q_o\, L^4)$) of the shear deformable propped-cantilever rectangular beam having a thickness-to-length ratio of 0.20, shear correction factor of 5 / 6 and Poisson's ratio of 0.3, with different combinations of number of nodes per element and total number of elements. These values are then compared with the corresponding analytical solution ($w^*_{max} = 0.6910$, Pakhare et al. [12]). Following four cases have been considered to arrive at the best combination of number of nodes per element and total number of elements for the subsequent electrostatic-elastic analysis:

1. The *TBT-SFE* with 6-noded element.
2. The *TBT-SFE* with 14-noded element.

3. The *TBT-SFE* with 20-noded element.
4. The *TBT-SFE* with 30-noded element.

The results for w^*_{max} for above-mentioned cases with different total number of elements is shown in Figs. 4 through 6.

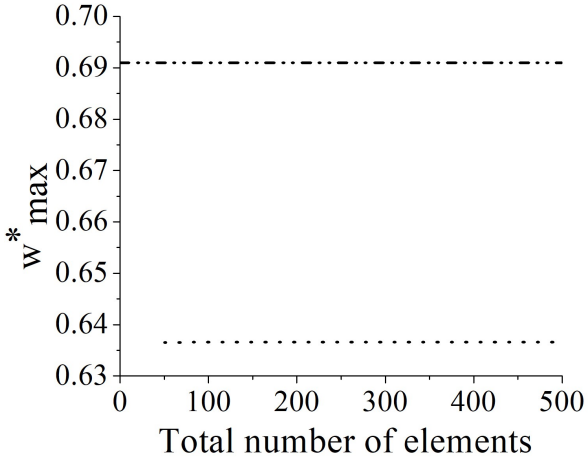

Fig. 4. The variation of the w^*_{max} with total number of elements for a 6-noded *TBT-SFE*, . . . for the *TBT-SFE* results and - . . - for the analytical result.

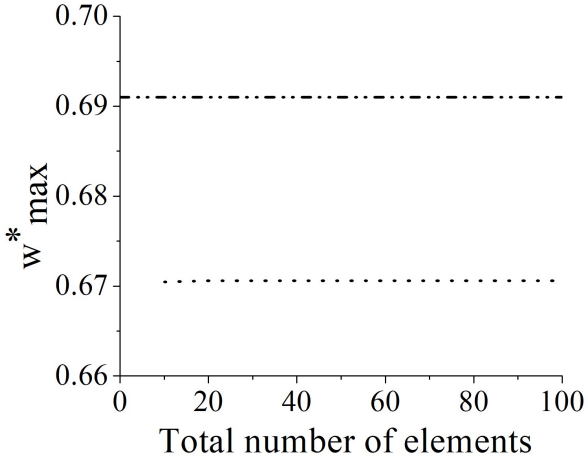

Fig. 5. The variation of the w^*_{max} with total number of elements for a 14-noded *TBT-SFE*, . . . for the *TBT-SFE* results and - . . - for the analytical result.

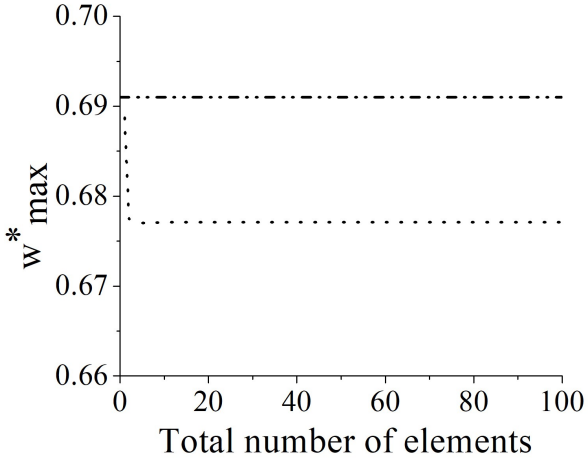

Fig. 6. The variation of the w^*_{max} with total number of elements for a 20-noded *TBT-SFE*, . . . for the *TBT-SFE* results and - . . - for the analytical result.

Authors have observed that a single *TBT-SFE* with 30-noded element gives $w^*_{max} = 0.6910$ which is the same as the corresponding analytical result reported in the literature. Hence a single *TBT-SFE* with 30-noded element is finalized to carry out the subsequent electrostatic-elastic analysis.

For the electrostatic-elastic analysis, following properties for the microbeam and the system are considered:

- The Young's modulus, $E = 169 \times 10^9$ Pa
- The Poisson's ration, $\mu = 0.3$
- The microbeam thickness, $h = 10$ µm
- The microbeam width, $b = 20$ µm
- The microbeam lengths, $L = 50, 100, 200, 1000$ µm
- The initial gap, $g_o = 1$ µm
- The permittivity of free space, $\varepsilon_o = 8.8542 \times 10^{-12}$ F / m

The pull-in voltage (V^*_{max}) and pull-in displacement (w^{**}_{max}) are defined as follows:

$$V^*_{\max} = \sqrt{\frac{\varepsilon_o\, b\, L^4}{2\, E\, I\, {g_o}^3}}\, V_{\max} \tag{16}$$

$$w^{**}_{\max} = \frac{w_{\max}}{g_o} \tag{17}$$

Following illustrative examples of microbeams are considered for the determination of their corresponding V^*_{max} and w^{**}_{max}:

- The illustrative example 1 (the *SS-SS* microbeam)
- The illustrative example 2 (the *C-F* microbeam)
- The illustrative example 3 (the *SS-C* microbeam)
- The illustrative example 4 (the *C-C* microbeam)

The values of V^*_{max} and corresponding w^{**}_{max} for illustrative examples 1 through 4 for microbeams having various values of the beam thickness-to-length ratio are presented in Tables 1 through 4 respectively. For the comparison purposes, these results are compared with corresponding results of the Bernoulli-Euler beam theory (*BEBT*) as reported by Jia et al. [13]. The percentage difference reported against results of the *BEBT* are calculated as follows:

% diff = ((The *BEBT* result / The *TBT-SFE* result) - 1) * 100

Table-1. The V^*_{max} and corresponding w^{**}_{max} for the illustrative example 1 (the *SS-SS* microbeam).

	V^*_{max}			
Theory	$h/L = 0.01$	$h/L = 0.05$	$h/L = 0.10$	$h/L = 0.20$
TBT-SFE [$]	3.7337	3.7127	3.6724	3.5399
BEBT [13]	3.7170	3.7170	3.7170	3.7170
	- 0.45 %	0.12 %	1.22`%	5.00 %
	w^{**}_{max}			
Theory	$h/L = 0.01$	$h/L = 0.05$	$h/L = 0.10$	$h/L = 0.20$
TBT-SFE [$]	0.3897	0.3913	0.3917	0.3915
BEBT [13]	0.3913	0.3913	0.3913	0.3913
	0.41 %	0.00 %	- 0.10 %	- 0.05 %

[$] A shear correction factor (κ) with a value 5 / 6 is used.

Table-2. The V^*_{max} and corresponding w^{**}_{max} for the illustrative example 2 (the *C-F* microbeam).

V^*_{max}

Theory	$h/L = 0.01$	$h/L = 0.05$	$h/L = 0.10$	$h/L = 0.20$
TBT-SFE [$]	1.3313	1.3113	1.2956	1.2693
BEBT [13]	1.3021	1.3021	1.3021	1.3021
	- 2.19 %	- 0.70 %	0.50 %	2.58 %

w^{**}_{max}

Theory	$h/L = 0.01$	$h/L = 0.05$	$h/L = 0.10$	$h/L = 0.20$
TBT-SFE [$]	0.4447	0.4463	0.4462	0.4458
BEBT [13]	0.4476	0.4476	0.4476	0.4476
	0.65 %	0.29 %	0.31 %	0.40 %

[$] A shear correction factor (κ) with a value 5 / 6 is used.

Table-3. The V^*_{max} and corresponding w^{**}_{max} for the illustrative example 3 (the *SS-C* microbeam).

V^*_{max}

Theory	$h/L = 0.01$	$h/L = 0.05$	$h/L = 0.10$	$h/L = 0.20$
TBT-SFE [$]	5.8138	5.7497	5.5972	5.1095
BEBT [13]	5.7979	5.7979	5.7979	5.7979
	- 0.27 %	0.84 %	3.59 %	13.47 %

w^{**}_{max}

Theory	$h/L = 0.01$	$h/L = 0.05$	$h/L = 0.10$	$h/L = 0.20$
TBT-SFE [$]	0.3938	0.3944	0.3943	0.3938
BEBT [13]	0.3944	0.3944	0.3944	0.3944
	0.15 %	0.00 %	0.03 %	0.15 %

[$] A shear correction factor (κ) with a value 5 / 6 is used.

Table-4. The V^*_{max} and corresponding w^{**}_{max} for the illustrative example 4 (the *C-C* microbeam).

V^*_{max}

Theory	$h/L = 0.01$	$h/L = 0.05$	$h/L = 0.10$	$h/L = 0.20$
TBT-SFE [$]	8.7308	8.3978	7.9330	6.8125
BEBT [13]	8.4035	8.4035	8.4035	8.4035
	- 3.75 %	0.07 %	5.93 %	23.35 %

w^{**}_{max}

Theory	$h/L = 0.01$	$h/L = 0.05$	$h/L = 0.10$	$h/L = 0.20$
TBT-SFE [$]	0.3966	0.3975	0.3970	0.3955
BEBT [13]	0.3971	0.3971	0.3971	0.3971
	0.13 %	- 0.10 %	0.03 %	0.41 %

[$] A shear correction factor (κ) with a value 5 / 6 is used.

From Tables 1 through 4, following observations can be made with regard to the pull-in voltage (V^*_{max}) and pull-in displacement (w^{**}_{max}) for the *SS-SS*, *C-F*, *SS-C* and *C-C* microbeams (illustrative examples 1 through 4 respectively):

1. The V^*_{max} gets reduced with increase in the beam thickness-to-length ratio as a result of beam transverse shear deformation effects. This effect gets magnified as the microbeam fixity moves from soft to hard *i.e.*, in order of the *C-F*, *SS-SS*, *SS-C* and *C-C* microbeams. In other words, the softening of thick microbeams as a result of the beam transverse shear deformation affects V^*_{max}.
2. Beam transverse shear deformation effects have little to no effect on the w^{**}_{max}.
3. The *BEBT* is unable to capture the softening behavior of shear deformable microbeams as its displacement field does not account for the transverse shear in the beam deformation. As a result, the V^*_{max} obtained by the *BEBT* remains overestimated for shear deformable microbeams. However, the w^{**}_{max} obtained by the *BEBT* and corresponding values obtained by the *TBT-SFE* are more or less the same for all values of the beam thickness-to-length ratio considered.

4. Concluding Remarks

In this paper, authors have developed the spectral finite element based on the Timoshenko beam theory (*TBT-SFE*) for the electrostatic-elastic analysis of electrostatically actuated narrow shear deformable microbeams, by taking a que from the work reported by Dileesh et al. (doi: 10.1115/ESDA2012-82536). However, authors have investigated the best combination of number of nodes per element and total number of elements to carry out the just-mentioned study. For this purpose, authors have first calculated results of the maximum beam transverse displacement, for a shear deformable propped-cantilever microbeam under the action of uniformly distributed transverse load, obtained by utilizing the developed *TBT-SFE* with different combinations of number of nodes per element and total number of elements. These results are then compared with corresponding analytical results reported in the literature to arrive at the best combination of number of nodes per element and total number of elements for the electrostatic-elastic analysis. This finalized *TBT-SFE* is then utilized to bring forward the effect that the beam transverse shear deformation has on pull-in parameters of narrow shear deformable microbeams with different fixity conditions. Obtained results are compared with corresponding results of the Bernoulli-Euler beam theory reported in the literature. To the best of authors' knowledge, such analysis where the Timoshenko beam theory is utilized for portraying the effects of the beam transverse shear deformation on pull-in parameters of electrostatically actuated narrow shear deformable microbeams is not previously reported in the literature.

Disclosures

Free Access to this article is sponsored by SARL ALPHA CRISTO INDUSTRIAL.

References

1. Zhang WM, Yan H, Peng ZK, and Meng G. Electrostatic pull-in instability in *MEMS* / *NEMS*: A review. Sensors and Actuators A: Physical, 2014; 214: 187-218.
2. Batra RC, Porfiri M, and Spinello D. Review of modeling electrostatically actuated microelectromechanical systems. Smart Materials and Structures, 2007; 16, R23.

3. Nathanson HC, Newell WE, Wickstrom RA, and Davis JR. The resonant gate transistor. IEEE Transactions on Electron Devices, 1967; 14: 117-133.

4. Ghugal YM, and Shimpi RP. A review of refined shear deformation theories for isotropic and anisotropic laminated beams. Journal of Reinforced Plastics and Composites, 2001; 20: 255-272.

5. Dileesh PV, Kulkarni SS, and Pawaskar DN. Static and dynamic analysis of electrostatically actuated microcantilevers using the spectral element method. ASME 11th Biennial Conference on Engineering Systems Design and Analysis, 2012; 11: 399-408.

6. Timoshenko SP. On the correction for shear of the differential equation for transverse vibrations of prismatic bars. Philosophical Magazine, 1921; 41: 744-746.

7. Timoshenko SP. On the transverse vibrations of bars of uniform cross-section. Philosophical Magazine, 1922; 43: 125-131.

8. Pakhare KS, Guruprasad PJ, and Shimpi RP. A single-variable first-order shear deformation nonlocal theory for the flexure of isotropic nanobeams. Journal of the Brazilian Society of Mechanical Sciences and Engineering, 2020; 42: 42.

9. Patera AT. A spectral element method for fluid dynamics: Laminar flow in a channel expansion. Journal of Computational Physics, 1984; 54: 468–488.

10. Komatitsch D, and Vilotte, J. The spectral element method: An efficient tool to simulate the seismic response of 2D and 3D geological structures. Bulletin of the Seismological Society of America, 1998; 88: 368–392.

11. Reddy JN. An introduction to the finite element method. McGraw-Hill Higher Education, 2006.

12. Pakhare KS, Guruprasad PJ, and Shimpi RP. A single-variable first-order shear deformation nonlocal theory for the flexure of isotropic nanobeams. Journal of the Brazilian Society of Mechanical Sciences and Engineering, 2020; 42: 42.

13. Jia XL, Yang J, and Kitipornchai S. Pull-in instability of geometrically nonlinear micro-switches under electrostatic and Casimir forces. Acta Mechanica, 2011; 218: 161–174.